Full Paper Transactions, SMiRT 28
Toronto, Canada, August 10-15, 2025

DROP LOADS ANALYSIS WITH ENERGY BALANCE METHODS AND FINITE ELEMENT EUROPLEXUS SOFTWARE

Anthony Darraba[1], Bastien Lafon[2]

[1] Fast dynamics specialist, Electricité de France (EDF), Lyon, France (anthony.darraba@edf.fr)
[2] Structural engineer, Electricité de France (EDF), Lyon, France (bastien.lafon@edf.fr)

ABSTRACT

A series of ten drop load experiments were performed with nearly perfectly rigid missiles, on Reinforced Concrete (RC) slabs. Two types of shear reinforcement were tested, leading to the conclusion that they had a very small influence on the slab damage. These tests, with a large range of impact energies, are exploited in this paper to assess the slab resistances, using both analytical and finite element methods.

Analytical calculations give a conservative assessment of the slab failure, for both punching and bending damages. Some assumptions are discussed, such as the impact diameter, the effective masses and the missile velocity after impact. A punching cone angle of 30° is recommended.

Finite element calculations give valuable information on the coupling between punching and bending damages. The punching damage area is well captured. From averaged maximum strains in lower bending reinforcement, a better failure estimate can be given than in analytical calculations.

INTRODUCTION

In Nuclear Power Plants (NPP), both in operation and in the decommissioning phase, many pieces of equipment are lifted and moved. The drop load event is addressed through a series of provisions on the design of handling devices and on human procedures. Nevertheless, some drop load scenarios can be analysed in terms of civil works consequences, and of functional consequences if needed, as complementary studies to the safety file. The resistance of civil works subjected to drop load scenarios can be quickly assessed with analytical calculations. These scenarios may involve nearly perfectly rigid missiles. Different methods can be suited to the hard impact of such missiles. In this paper, energy balance methods are applied to drop load tests on RC slabs. The tests lead to different punching and bending damage levels. Finally, finite element calculations are performed with the EUROPLEXUS software.

DROP LOAD EXPERIMENTS

A series of ten drop tests was performed in 2013 in the Montagnole test facility (IFFSTAR, now G. Eiffel University). The common parameters of all the tests were the spherical missile shape, the impacted slab thickness of 300 mm, the bending reinforcement ratio of 13,4 cm²/m (Ø16 @ 150 mm each way each face), the shear reinforcement ratio of 50 cm²/m² (Ø12 @ 150 mm), the concrete compression strength specified as C60/70 and the slab supports. Each slab is placed on two steel bars of 15 mm width, along two opposite edges, the two other edges being free. The steel bars are anchored to four rigid concrete blocks anchored to the ground (see Figure 2). The supporting then corresponds to a one way simply supported condition.

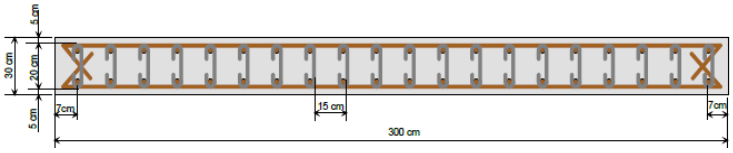

Figure 1. Reinforcement of the impacted slabs – Case of stirrups for the shear reinforcement

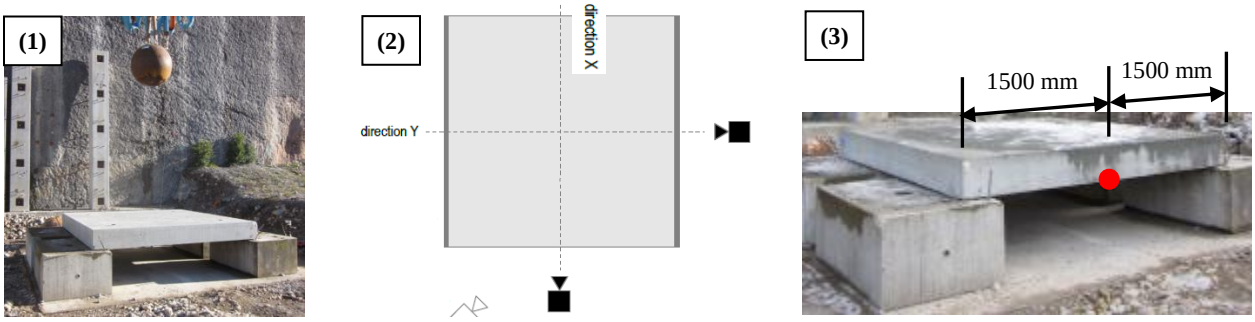

Figure 2. Test overview (1), fast cameras setup (2), reference point for the displacement measurement (3)

The initial objective of these tests was to compare drop load tests on slabs in which shear reinforcement is composed of either stirrups or T-headed bars, all other parameters being fixed. Five couples of tests were performed, resulting in ten tests. The Table 1 summarizes the main parameters that are modified between the tests. The concrete compression strength measured on 150 mm cubic specimen at the time of each impact test is given. The scattering of concrete strengths is low. Besides, after tests 3-4, permanent strains were observed on the missile, composed of concrete surrounded by a steel shell. In subsequent tests 5-10, a spherical steel missile was used. No visible missile damage was then observed after these tests.

Table 1: Specific parameters for each drop load test (ST=stirrups, TH= T-headed bars)

Test	1	2	3	4	5	6	7	8	9	10
Missile mass [kg]	115		548		2500		2500		2500	
Drop height [m]	7.49		10.02		5.01		2.53		10.02	
Missile diameter [m]	0.42		0.73		0.86		0.86		0.86	
Shear reinf. type	ST	TH	TH	ST	ST	TH	TH	ST	ST	TH
Concrete compression strength [MPa]	73.2	75.6	71.0	69.4	68.8	69.8	75.6	73.2	67.5	69.7

After the tests, it was pointed out that the displacement of the slab, the cracks in the slab cross sections and the overall damage in the punching cone area were very similar for each couple of tests. Therefore, the type of shear reinforcement bars had a very small influence on the slab damage.

Slab Damage

As a result of the very different impact energies in the tests, the slabs damages range from negligible to high bending and punching damage, without failure. All the slabs were cut after each test, along X and Y directions, and cracks highlighted with water. The following conclusions are drawn:

- Tests 1/2: no visible crack, no damage. The slab is reused in Tests 8/7 respectively,
- Tests 3/4: A few punching cracks at the cone boundary and bending cracks initiated on the impact opposite side, on cross sections, micrometre wide and not visible. In both bending and punching, the slab is close to entire integrity,
- Tests 7/8: Small concrete cover pieces detached in the punching cone. Radial bending cracks on cross sections initiated on the rear side, 0.1 to 1.0 mm wide, the bending damage is considered as

low. Despite the beginning of scabbing, that could be due to the hard impact overpressures, there are few cracks in the punching cone area. The cone is hard to identify and far from being detached,

- Tests 5/6: Scabbing on the cone surface. Visible radial bending cracks outside the punching cone. The main bending cracks are along the 2 symmetry planes of the slab. Punching damage is the main damage mode, looking at the cross sections and the rear face, with one lower rebar broken in the Y direction in the punching cone of test 5,
- Tests 9/10: Many cracks in the punching cone. Bending cracks clearly opened along the plane of symmetry parallel to the supports (X direction). Two lower bending bars are broken (in the Y direction) in the punching cone of test 10. High bending and punching damage.

ANALYTICAL CALCULATIONS

The perforation thickness under hard impact can be estimated with perforation formulas, such as the CEA-EDF formulas, see RCC-CW (2023). It was found in hard impact tests at velocity in the order of 100 m/s, that the bending and the shear reinforcements have a minor influence on the slab resistance, see Galan et al. (2022).

When the missile velocity is low, hard impact can also lead to punching, with almost no missile penetration in the RC slab. A punching cone is observed, as in soft impact tests at higher velocities, if the punching resistance is exceeded. The work done on such impact tests, which lead to a punching cone, concluded that both bending and shear reinforcements have a significant influence on the slab resistance, on top of the concrete strength, see Darraba et al. (2022).

As an alternative to force methods, energy balance methods can be applied to hard impacts at low velocities. These methods consist in assessing the punching and bending resistances. They are introduced in the RCC-CW civil works code. The two failure modes are verified independently.

Punching Verification

The method is derived from the so-called CEB model detailed in CEB (1988). The punching cone is represented by a mass. This mass is linked to a non-linear spring describing the punching response of the slab, see Figure 3. The contributions of the concrete, through its tensile strength along the expected cone boundaries, the stirrups (until failure in tension) and the lower bending reinforcement, developing large plastic strains in the cone area, are considered. The surrounding part of the slab, which mass is *Mb*, is also described with a non-linear spring. It is used solely for the bending capacity assessment of the energy balance method, not for the punching one.

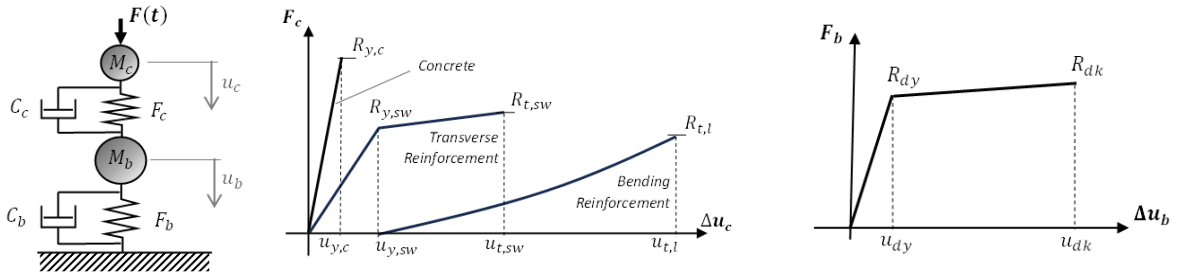

Figure 3. Force-displacement modelling of the punching cone (M_c, F_c) and of the surrounding bending slab (F_b, M_b) subjected to an impact force *F(t)*

The punching resistant energy, or punching capability energy, corresponds to the maximum energy that can be dissipated through the displacement of the punching spring:

$$E_{cap,punching} = E_{cap,concrete} + E_{cap,transverse\ reinf} + E_{cap,bending\ reinf} \quad (1)$$

It can be demonstrated that (1) leads to the following equation:

$$E_{cap,punching} = \frac{R_{y,c}.u_{y,c}}{2} + \frac{R_{y,sw}.u_{y,sw}}{2} + \frac{R_{y,sw}+R_{t,sw}}{2}.\left(u_{t,sw} - u_{y,sw}\right) + \frac{R_{t,l}.u_{t,l}}{4} \quad (2)$$

Where all the parameters are defined in Figure 3 and can be calculated with the help of RCC-CW. The punching cone geometry must be defined, through the missile radius R_p and the punching cone angle α. In soft impact punching tests at roughly 100 m/s, the angle proposed in RCC-CW of 40° with respect to the slab surface, for flat slabs without prestressing, turned out to be well suited whatever the damage level, see Darraba et al. (2022). Drop load tests from the literature and from the experiments presented in this paper were analysed. It was concluded that an angle of 30° is well suited for drop loads. This is a good estimate of the main punching crack, in the four tests of this paper where the punching cone is created, i.e. in tests 5/6 and 9/10.

The spherical shape of the missile makes it complicated to derive a missile radius R_p. After each test, the diameter of the damaged area in the slab front face was measured. The punching cracks on the slab cross sections after the experiments are coming from this damaged area. The missile radius R_p is therefore considered as half the measured impact diameter.

Besides, considering the missile undeformed after impact, the penetration depth in the slab is calculated based on the missile diameter and the front face damage crater diameter. These values are summarized in Table 2. All penetration depths are well below the concrete cover of 50 mm, as observed after tests. For tests 1/2, there is no damage on the front face. In the objective to consider a non-zero missile diameter for calculations, the same penetration of 4 mm is assumed in tests 1/2 as in tests 3/4. The impact diameter for tests 1/2 is deduced based on the actual missile diameter.

The concrete material properties are defined from measured compression strengths (see Table 1). Both bending and shear reinforcements are made of B500B bars. A tensile yield stress for rebars of 500 MPa is considered. The strain at maximum stress ε_{uk} is 5 %, as certified by the steel manufacturer. The same value is considered for the failure strain. The maximum stress considered is 540 MPa. For both initial yield stress and maximum stress, a Dynamic Increase Factor of 1.1 is applied to account for tensile strain rates of about 1 s^{-1}- 10 s^{-1} , according to simulations presented in the following.

Conservation of momentum before and after the impact provides a relation between the incident velocity of the missile and the velocity of the equivalent missile/concrete punching plug system after impact. The energy that the slab should be able to handle during the impact is the kinetic energy of the equivalent missile/concrete plug system, namely the incident effective punching energy:

$$E_{p,effective\ punching} = \frac{1}{1+\frac{M_c}{M_p}}.E_p \quad (3)$$

Where E_p is the incident kinetic energy of the missile, M_c is the mass of the concrete cone and M_p is the mass of the missile. The calculation of M_c requires the punching cone angle α, previously defined as 30°. The work due to the missile weight is neglected.

The punching calculations are presented in Table 2. To simplify, only the first test is considered for each couple of tests. Results are presented for increasing incident energy.

Table 2. Analytical punching calculations

Test	1	3	7	5	9
Kinetic incident energy [kJ]	8	54	62	123	246
Impact diameter [m]	0.08	0.11	0.14	0.19	0.22
Penetration in the slab [m]	0.004	0.004	0.005	0.011	0.015
Punching cone mass [kg]	266	285	306	349	377
$1/(1+M_c/M_p)$	0.30	0.66	0.89	0.88	0.87
$E_{p,effective\ punching}$ [kJ]	2.5	35	55	108	214
$E_{cap,punching}$ [kJ]	49	52	55	60	64
Punching Ratio	**19**	**1.5**	**1.0**	**0.56**	**0.30**

It can be observed that the reduction of the initial kinetic energy to the effective one is mainly significant for the experiments with low missile mass relative to the punching cone mass i.e. tests 1-3. The punching ratio is high in test 1, and still higher than 1 in test 3, despite the small impact diameter considered. If the 15 mm penetration depth from test 9 is considered, the consequently increased impact diameter would improve the ratios to 25, 1.9 and 1.2 respectively for tests 1, 3 and 7. It does not change dramatically the punching ratios. The lower bending reinforcement contributes to 70-75 % in the whole energy capacity. The remaining part comes from the shear reinforcement. The drawback of this method is the negligible concrete contribution, which is not realistic for the punching cone damage mode, see Darraba et al. (2022).

The punching failure would then be expected for impact energy close to test 7. This experiment shows few inclined cracks as mentioned earlier. The method is therefore conservative with respect to a high damage assessment, and it is more suited to design slabs with low to moderate damage.

Bending Verification

Based on Figure 3, the bending energy capacity of the slab can be written as:

$$E_{cap\ bending} = \frac{R_{dy}.u_{dy}}{2} + \frac{R_{dy}+R_{dk}}{2}.\left(u_{dk} - u_{dy}\right) \quad (4)$$

Where all the parameters are defined in Figure 3 and can be calculated with the help of RCC-CW. u_{dy} and R_{dy} are calculated from the elastic theory of plates or beams. The ultimate load R_{dk} is derived from the yield lines theory, see Johansen (1962).

EDF performed yield lines calculations on different slab conditions (various span lengths to width ratio, edges clamped or simply supported), to verify that the shape of the failure mechanism is consistent with what is expected from the theory and from experiments, see Figure 4.

4 edges clamped 7m x 3m ***(a)*** | *4 edges simply supported 7m x 3m* ***(b)*** | *4 edges simply sup. 3 m x 3 m* ***(c)*** | *2 edges clamped or simply supported slab* ***(d)***

Figure 4. Yield lines selected pattern for different slabs span to width ratios and supporting conditions

For each failure mechanism, the work associated to the external loads is equal to the dissipated energy through the yield lines rotation. The ultimate capability of the slab is the one leading to an ultimate yield line rotation, calculated from the slab Moment-Curvature relationship and its geometry. Due to the conservation of momentum, the bending kinetic energy transmitted to the slab, namely the effective incident bending energy, reads:

$$E_{p,eff\ bending} = \frac{1+\frac{M_{eff2}}{Mp}}{\left(1+\frac{M_{eff1}}{Mp}\right)^2}.E_p \tag{5}$$

Where m_{eff1} is the effective mass of first order of the slab and m_{eff2} is the effective mass of second order:

$$M_{eff1} = \frac{1}{u_{1m}}.\iint_{slab}\mu(x,y).u_1(x,y).dx.dy \tag{6}$$

$$M_{eff2} = \frac{1}{u_{1m}^2}.\iint_{slab}.\mu(x,y).u_1^2(x,y).dx.dy \tag{7}$$

Where u_1 is the displacement of the slab at point of coordinates (x,y) due to the impact load, u_{1m} is the mean displacement of the slab below the missile due to the impact load and μ is the mass per unit of surface at point of coordinates (x,y). A non-linear finite element calculation can give precisely M_{eff1} and M_{eff2}, as the deformed shape must be known. Nevertheless, a common simplification is to compute them assuming that the deformed shape is identical to the linear elastic one. It is here performed with this assumption, with the help of a python script. M_{eff1} and M_{eff2} are better assessed in finite element calculations in this paper. They confirm that values given in Table 3 can be used conservatively.

The bending calculations are summarized in Table 3. From the maximum displacement measured at the slab free edge, see Figure 2 and Figure 6, the support rotation is also given. This latter can be compared to simple bending criteria given for instance in IAEA (2018).

Table 3. Analytical bending calculations

Test	1	3	7	5	9
Kinetic incident energy [kJ]	8	54	62	123	246
Maximum displacement [m]	0.004	0.016	0.035	0.057	0.104
Support rotation [°]	0.2	0.6	1.3	2.2	4.0
Effective mass M_{eff1} [kg]	4261	4261	4262	4263	4263
Effective mass M_{eff2} [kg]	3312	3312	3312	3314	3314
$E_{p,eff\ bending}$ [kJ]	0.2	4.9	19.7	39.0	78.1
$E_{cap,bending}$ [kJ]	30.0	30.7	31.4	32.4	33.0
Bending Ratio	**150**	**6.3**	**1.6**	**0.83**	**0.42**

It is noticed that the yield lines calculation leads to the same preferred failure mechanism for all the tests, with a single crack between supports, see Figure 4 (d). The bending ratio is high in tests 1 and 3, and becomes lower than 1 for tests 5 and 9. Values of about 0.4 are therefore associated to significant cracks opening on the slab rear face, as observed in test 9. As for punching, the method does not lead to an accurate failure estimate.

One assumption made to establish equation (5) is that the missile and slab velocities after impact are identical. This assumption is justified for soft impacts. For hard impacts, it may be verified with the elastic shocks' theory, introducing a restitution coefficient e. It is defined as the ratio of the missile/slab relative velocity after impact over the one before impact (8). Using the conservation of momentum provides an alternative expression of the restitution coefficient (9):

$$e = \left|\frac{V_{S,1} - V_{P,1}}{V_{P,0}}\right| \quad (8) \quad \xrightarrow{Conservation\ of\ momentum} \quad e = \left|\left(1 + \frac{M_{eff1}}{M_P}\right).\frac{V_{S,1}}{V_{P,0}} - 1\right| \quad (9)$$

Where $V_{P,0}$ is the missile velocity before impact, $V_{P,1}$ is the missile velocity after impact and $V_{S,1}$ is the slab velocity after impact. A zero value corresponds to a perfectly plastic shock ($V_{S,1} = V_{P,1}$). On the opposite, a value of 1 is an elastic shock in which the kinetic energy of the missile/slab system is conserved.

From the slab's displacement measured during the test (see Figure 6), the slab's mean velocity after impact can be derived. Using the effective mass of order 1 previously calculated (see Table 3), the restitution coefficient e and then the missile velocity after impact can be estimated, see Table 4:

Table 4. Restitution coefficient in the elastic shocks' theory

Test	1	3	7	5	9
Slab mean velocity after impact [m/s]	0.4	1.8	2.8	3.8	5.1
Restitution coefficient e [-]	0.38	0.13	0.07	0.04	0.02
Missile velocity after impact [m/s]	-4.2	0.02	2.3	3.4	4.9

The restitution coefficient ranges from 0.4 to 0.1 for tests ranging from no damage (missile rebound, as observed on fast cameras) to very low damage, respectively in tests 1 and 3. The coefficient is close to 0 for tests with bending damage. On the video footages from tests 5 and 9, the missile follows the slab during a significant time relatively to the slab displacement duration. It is concluded that the assumption of e=0 is valid with the objective to assess the slab capacity until failure.

FINITE ELEMENT CALCULATIONS

Where analytical methods predict slab failure in tests with missile incident energy of 123 kJ and higher for bending, or higher than 62 kJ in punching, finite element calculations may provide more accurate results on the slab damage. A 3D finite element model is built to compute different cases of the drop tests series with the EUROPLEXUS software. The slab modelling is basically the same as in Darraba et al. (2024). The steel bars (in green on Figure 5) are modelled with fully integrated solid elements. The missile, the slab and the concrete supporting blocks are modelled with under-integrated solid elements. Linear elastic material model is associated to the missile, the steel bars and the blocks. The slab material model is the Damage Plastic Dynamic Concrete (DPDC) model. It is described more in details in Zhang (2025).

Reinforcements are modelled using beam elements with a trilinear material model. Both shared nodes and constraint coupling were investigated for the reinforcement's links to concrete. As calculation results were similar with big differences in the computation time, the shared nodes modelling was chosen.

The parameters from Zhang (2025) are considered for the DPDC modelling, including the control of the hourglass modes by means of an added viscous force (coefficient of 0.1), and the three erosion criteria on the volumetric strain ε_V (elements are deleted when $\varepsilon_V > 0.8$), on ductile damage d^d under compression (elements are deleted when $d^d > 0.9$) and on the shear strain depending on the confinement ratio. This latter

criterion follows the theory exposed in Özen and Fedoroff (2022). However, in the drop tests, the missile penetration in the slab is very low. The perforation damage mode of RC slabs subjected to hard impact at velocities of about 100 m/s, is not relevant in this paper. It was verified that this criterion can be removed, without any change in the results, as no element is deleted in the punching cone. The main interest is then to verify that the shear criterion is not suited to drop loads, where the missile does not penetrate significantly into the slab. The two other erosion criteria are useful to delete highly distorted slab elements under the missile nose. In rebars, no erosion criterion is used, except as a sensitivity analysis further mentioned.

A contact interface between the slab and the two supporting steel bars is computed. The two steel bars are connected to four rigid concrete blocks anchored to the lab base slab, see Figure 2.

Three element sizes of cubic concrete elements were considered for the whole slab: 30 mm, 19 mm and 15 mm (with an aspect ratio close to 1). These mesh sizes lead to 10, 16 and 20 elements in the slab thickness respectively, and 2, 3 and 4 elements in the concrete cover up to the rebar centre, which is in good agreement with the 50 mm thick concrete cover at the rebar external surface. The following figure shows the mesh finally used, with 16 concrete elements in the slab thickness. The mesh sensitivity pointed out that this mesh is refined enough based on displacements and cone damage. The missile mesh was chosen accordingly, so that the mesh size in the impact area is similar for the missile and the slab. The rebar mesh has the same size as the concrete elements size.

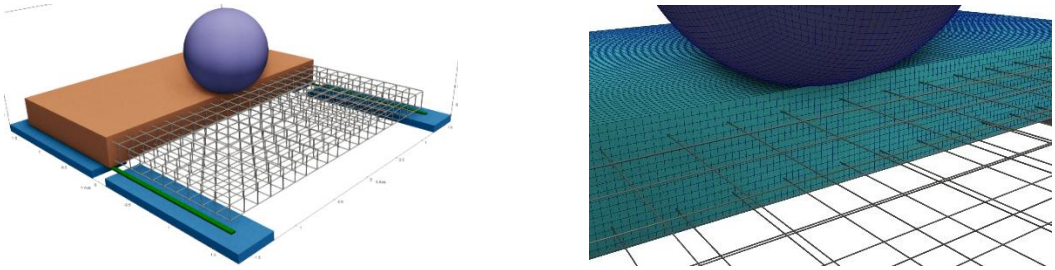

Figure 5. Finite element model overview for tests 5 and 9 (on the left), zoom in on the mesh (on the right)

The following figure compares the displacements from measurements and calculations. The displacement measurement in test 9 did not work. The displacement evolution at the slab free edge is well captured in the finite element calculation. The maximum displacement is under-estimated by 10-20 % approximately for tests 7-5-9. With only one displacement measurement, from a fast camera close to the slab, this difference is not further analysed.

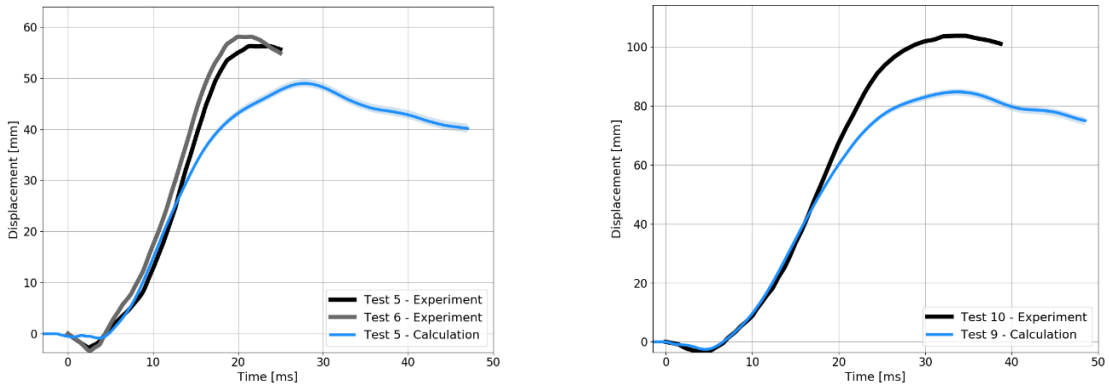

Figure 6. Displacement over time in Test 5 (on the left) and Test 9 (on the right)

From the non-linear displacements computed, the effective masses defined in (6) (7), used in analytical bending calculations, can be calculated. The displacements at the slab mid plane are considered.

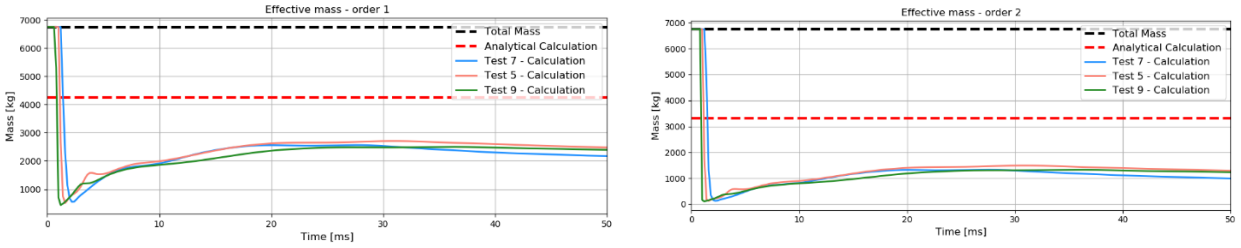

Figure 7. Effective mass of first order (on the left) and of second order (on the right)

The analytical masses are overestimated compared to the ones calculated from the non-linear deformed shape. It can be explained by the higher displacements localized around the punching cone, in the latter case. The analytical calculation does not capture it, the linear elastic deformed shape being approximated by that of a beam-like slab, simply supported. This leads to higher global displacements over the slab's width and consequently higher effective masses.

The following figure shows the maximum principal compressive strain in concrete and tensile strain in the lower bending and in shear reinforcements, at the maximum displacement time. For the bending bars, the plotted strains are averaged on a length equal to d, the effective thickness, corresponding to a distance of 250 mm from the impact face to the lower reinforcement. For the mesh size considered, this means strains, for each steel element of the lower bending reinforcement in the Y direction, are averaged over 13 elements (6 elements on each side of the considered one, hence corresponding to a 244 mm distance).

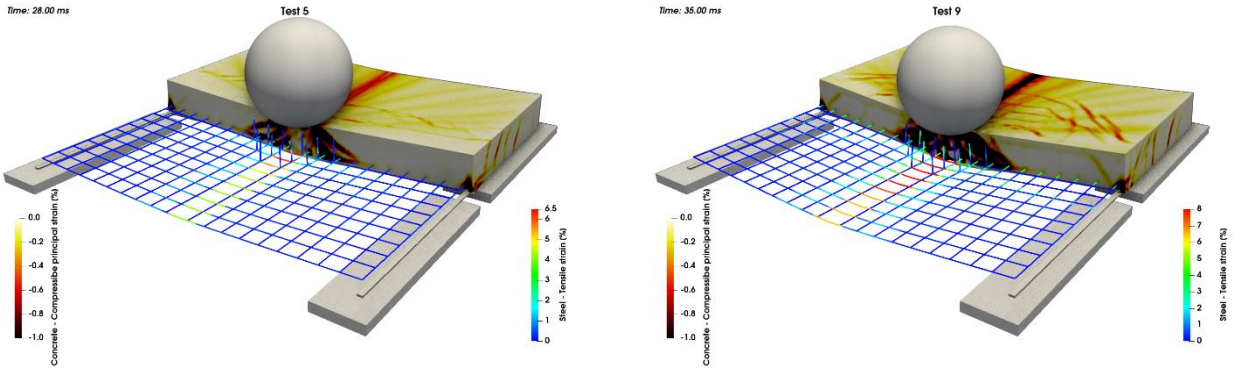

Figure 8. Maximum principal compression strain in concrete and averaged tensile strain in rebars – Test 5 (on the left, t=28 ms) and Test 9 (on the right, t=35 ms)

It appears that the punching cone damage is well captured by the concrete compression strain post-processed (a lower bound of -1% is defined in the scale). The maximum averaged tensile strains in the lower rebars are higher than 5 % in the punching cone area for test 5 and 9. Outside the cone, they are lower than 5% for test 5 but higher for test 9. This value of 5 %, proposed for instance in IAEA (2018), is then considered as a good basis for a failure criterion, when compared to the damage previously pointed out in the experiments. Lower strains are calculated in the shear reinforcement, basically under 1.5 % for test 5 and under 2.5 % for test 9, with local maximum values of 2.5 % for test 5 and 3.5 % for test 9.

If an erosion criterion is applied on the tensile strain of the rebars, the slab in both tests 5 and 9 reaches bending failure. The strain in one element of each lower rebar in the Y direction reaches a very

high value. It is then not possible to correctly correlate the slab damage, in both tests. An erosion criterion based on the averaged tensile strain, showed on Figure 8, would be more suited.

Finite elements calculations give insights on the coupled punching and bending damages. If the 5% criterion on the tensile strain is applied to the averaged strains of the lower reinforcement between supports (Y direction), bending failure of the slab would be predicted in test 9 but not in test 5, which would better correlate the experiments. Punching damage is in good agreement with the tests, more predominant than the bending one in tests 5 and 9. Moreover, simulations provide better estimates of effective masses, taking into account localised higher displacements in the punching cone. This illustrates some conservatisms of simplified analytical methods.

CONCLUSION

A series of ten drop load experiments were performed with nearly perfectly rigid missiles, on RC slabs. Two types of shear reinforcement were tested, leading to the conclusion that they had a very small influence on the slab damage. These tests, with a large range of impact energies, are exploited in this paper to assess the slab resistances, using both analytical and finite element methods.

The basic principles and criteria are reminded for analytical calculations. Some assumptions are discussed, such as the impact diameter, the effective masses and the missile velocity after impact. A punching cone angle of 30° is recommended based on tests and calculations results. The calculations provide a fast assessment of the slab damage, with conservative estimates of the slab failure. It is particularly true for punching, where a ratio of one is associated with a low to moderate damage in the test, with few punching cracks in the slab cross sections. It can be explained by the negligible contribution of concrete to the resistance in the energy balance method. Finite element calculations give valuable information on the coupling between punching and bending damages. The punching damage area is well captured. From averaged maximum tensile strains in the lower bending reinforcement between supports, a better failure estimate can be given compared to analytical calculations.

Further experiments may be conducted with cylindrical or cubical shaped missiles, and other supporting conditions could be investigated: two-way supported slabs, and close to clamped condition.

REFERENCES

CEB (1988). *Concrete structures under impact and impulsive loading*, Comité Euro-international du Béton, 1988

Darraba A., Lafon B., Galan M., Schneeberger C. (2022). “Verification of punching damage of reinforced concrete slabs under soft impact with RCC-CW punching resistance”, *SMiRT26 - Berlin/Potsdam, Germany. 2022. IASMiRT*

Darraba A., Ghadimi Khasraghy S., Lafon B., Wilding B. (2024). “Effect of impact location on the punching shear resistance of a concrete wall: analytical and numerical interpretation with EUROPLEXUS and LS-DYNA”, *SMiRT27 - Yokohama, Japan. 2024. IASMiRT*

Galan M., Darraba A. (2022). “A synthesis of the VTT IMPACT project phases II and III”, *SMiRT26 - Berlin/Potsdam, Germany. 2022. IASMiRT*

IAEA (2018). “Safety Aspects of Nuclear Power Plants in Human Induced External Events : Assessment of Structures”, Safety Report Series No. 87, International Atomic Energy Agency, Vienna, 2018

Johansen, K. W. (1962). *Yield-line theory*, Cement and Concrete Association, London, UK

Özen K., Fedoroff A. (2022). “Simulation of pre-stressed slabs using ABAQUS CDP material model”, *SMiRT26 - Berlin/Potsdam, Germany. 2022. IASMiRT*

RCC-CW (2023). *RCC-CW 2023 Edition – Rules for design and construction of PWR nuclear civil works*, AFCEN ed.

Zhang Y. (2025). “3D modelling and simulation of impacts on reinforced-concrete structures with EUROPLEXUS”, *SMiRT28 - Toronto, Canada. 2025. IASMiRT*